biophysica

MDPI

Article

Assessing the Effects of Photodynamic Therapy with Exogenous PpIX and Rose Bengal in an Ex Vivo Non-Muscle-Invasive Bladder Cancer Low-Grade pTa Model

Dominik Godlewski [1], Michał Osuchowski [2], Tomasz Kubrak [3,*], Agnieszka Przygórzewska [4], Sara Czech [4] and David Aebisher [5,*]

1 Medical Center in Łańcut, 37-100 Łańcut, Poland; remediumplus@o2.pl
2 Department of Patomorphology, Faculty of Medicine, Collegium Medicum, 35-959 Rzeszów, Poland; mosuchowski@ur.edu.pl
3 Department of Biochemistry and General Chemistry, Faculty of Medicine, Collegium Medicum, University of Rzeszów, 35-310 Rzeszów, Poland
4 English Division Science Club, Faculty of Medicine, Collegium Medicum, 35-959 Rzeszów, Poland; agnieszkaprzygorzewska@gmail.com (A.P.); sc126240@stud.ur.edu.pl (S.C.)
5 Department of Photomedicine and Physical Chemistry, Faculty of Medicine, Collegium Medicum, University of Rzeszów, 35-310 Rzeszów, Poland
* Correspondence: tkubrak@ur.edu.pl (T.K.); daebisher@ur.edu.pl (D.A.)

Abstract

Herein, we report a simple procedure regarding the photodynamic therapy (PDT) treatment as a minimally invasive modality for treating superficial bladder cancer that utilizes a photosensitizer, light, and oxygen to generate cytotoxic reactive oxygen species (ROS). This study evaluates the histopathological and morphological changes induced by PDT in an ex vivo model of low-grade (LG) pTa non-muscle-invasive bladder cancer (NMIBC). We investigated the efficacy of exogenous protoporphyrin IX (PpIX) and Rose Bengal (RB) by incubating tissue samples (n = 30) with an oxygen-saturated solution of PpIX (1–3 mM) or RB (0.3–0.5 mM) for one hour. Since the criticism of using frozen tissue in research already exists, this framing explains how to mitigate those limitations. Thus, we use oxygen-saturated solutions PpIX and oxygen-saturated solutions of RB. We discussed a few aspects related to the use of frozen tissue in PDT. Frozen tissue preserves lipids critical for assessing membrane damage and maintains higher levels of metabolic markers like antioxidant molecules like glutathione and more likely lack factors such as metabolic activity, intact cell membranes, and oxygenation. It is critical to differentiate between "artifactual" changes and the "pathological" death of cells. Thus, we used histopathological microscopy observation typically used in daily clinical investigations to characterize cells before and after PDT. Following irradiation with the light dose of 72 J/cm^2 (410 nm or 532 nm at 300 mW for 15 min), hematoxylin–eosin staining revealed concentration-dependent apoptotic changes, including chromatin condensation, pyknosis, and nuclear fragmentation. While both agents induced cell death, RB demonstrated faster and more intense cytotoxicity than PpIX. These findings provide microscopic evidence of PDT-induced tumor destruction and suggest that RB is a potent candidate for further preclinical evaluation. At 410 nm (deep blue/violet), light penetration in biological tissue is very shallow, typically only around 0.3 to 1 mm; therefore, in a 2 mm thick tissue sample, most of the light would be absorbed within the first millimeter, with minimal light reaching the full depth of tissues. In this protocol, the generated ROS is used to destroy tumor tissue by attacking the cellular microenvironment directly. This led to immediate membrane disruption and lipid peroxidation. The proof-of-concept is an early-stage study designed to verify that a PDT treatment is feasible, safe, and biologically active in an ex vivo model of LG pTa NMIBC.

Check for updates

Academic Editor: Herbert Schneckenburger

Received: 27 February 2026
Revised: 5 April 2026
Accepted: 15 April 2026
Published: 8 May 2026

Copyright: © 2026 by the authors. Licensee MDPI, Basel, Switzerland. This article is an open access article distributed under the terms and conditions of the Creative Commons Attribution (CC BY) license.

Keywords: photodynamic therapy (PDT); protoporphyrin IX (PpIX); Rose Bengal (RB); non-muscle-invasive bladder cancer (NMIBC); histopathology; apoptosis; reactive oxygen species (ROS)

1. Introduction

Bladder cancer is one of the most common malignancies worldwide. According to global data, it is the seventh most common cancer in men and the tenth in both sexes. Moreover, it is the thirteenth leading cause of cancer-related deaths worldwide [1]. The most common bladder cancer, which accounts for more than 90% of all bladder cancers in the population of industrialized countries, is urothelial carcinoma of transitional epithelial origin [2]. Clinically, a distinction is made between non-invasive forms (NMIBC), confined to the mucosa or lamina propria, with a high risk of recurrence, and invasive forms (MIBC), infiltrating the bladder muscle with a risk of metastasis and a much worse prognosis [3]. The decisive advantage in incidence is NMIBC, which accounts for ~75% of newly diagnosed cases of bladder cancer [4]. The classic NMBIC histopathological division, based on the depth of infiltration (TNM system), distinguishes three basic categories of lesions: carcinoma in situ (Tis/CIS), pTa tumors and pT1 tumors. Carcinoma in situ is a multifocal, flat, high-grade lesion confined exclusively to the epithelial layer of the mucosa, without papilla formation or infiltration of the deeper layers of the bladder wall. Tumors of pTa are papillary, superficial tumors confined to the epithelium that do not cross the basement membrane and do not show signs of invasion. In contrast, pT1 tumors are characterized by infiltration of the submucosa (lamina propria), but stop before the muscularis propria layer [5]. The pTa tumors comprise approximately 70% of NMIBC cases [6], and of these, the vast majority (approximately 84%) are low-grade (NMIBC pTa LG), characterized by low malignancy [7]. Although NMIBC pTa LG is considered a relatively benign disease, standard transurethral treatment (TURBT) is associated with a high recurrence rate. Jeong et al., in a cohort of 1067 patients with pTa tumors, noted that up to 60–70% of patients experience recurrence after treatment [8]. One method with promising clinical results in the treatment of NMIBC pTa LG, when standard therapies have failed, is photodynamic therapy (PDT) [9].

Photodynamics is an interdisciplinary field of science that combines elements of physics, chemistry and biology to use light, light-sensitive substances (photosensitizers, PSs) and oxygen to induce chemical and biological reactions. Its applications in medicine include both diagnostics and therapy, gaining increasing importance in the treatment of cancer and other diseases. The basic mechanism of photodynamics is the interaction of light of a specific wavelength with a photosensitizer, which, upon activation, enters an excited state and generates reactive oxygen species (ROS). These highly reactive molecules cause local tissue damage, including cancer cell death, with minimal impact on surrounding healthy tissues [10]. Due to this precise selectivity, PDT is used in the treatment of various cancers, such as skin cancer [11], head and neck cancer [12], gastrointestinal cancer [13,14], lung cancer [15], prostate cancer [16] or bladder cancer [17,18], as well as in the treatment of dental diseases and bacterial infections [19]. As mentioned earlier, PDT is based on three key components: a PS, visible light of an appropriate wavelength and the presence of molecular oxygen in the tissue. The interaction of these elements leads to the generation of reactive oxygen species (ROS), such as singlet oxygen ($^1O_2$), hydrogen peroxide (H_2O_2), hydroxyl radical (OH·) and superoxide anion (O^{2-}), which are responsible for the destructive effect on cancer cells [20,21]. The photodynamic mechanism is based on two main photochemical pathways, called Type I and Type II mechanisms. In the Type

I process, the photosensitizer reacts with molecules in the environment, leading to the formation of free radicals and reactive oxygen species [22]. In the Type II mechanism, the energy of the excited photosensitizer is transferred to molecular oxygen, which results in the formation of singlet oxygen, a key cytotoxic factor [23]. Both mechanisms can act simultaneously, but their dominance depends on the properties of the photosensitizer, the concentration of oxygen in the tissue, and light parameters such as wavelength and intensity [24]. ROS generated as a result of PDT exhibit multidirectional effects on cancer cells, leading to apoptosis, autophagy, or necrosis [25,26]. The apoptosis process is often initiated by mitochondrial damage and the release of cytochrome c, which activates a signaling cascade leading to controlled cell death. Although autophagy initially plays a protective role by recycling damaged organelles, under conditions of prolonged oxidative stress it can also contribute to cell death. Necrosis, in turn, is associated with direct damage to cell membranes by ROS, which results in the spillage of cell contents and the induction of a local inflammatory response. PDT also affects the tumor microenvironment, causing damage to blood vessels, which limits the supply of oxygen and nutrients to the tumor. In addition, PDT can stimulate the immune system by releasing tumor antigens, which leads to the activation of an antitumor response [27]. The mechanism of action of PDT is shown in Figure 1.

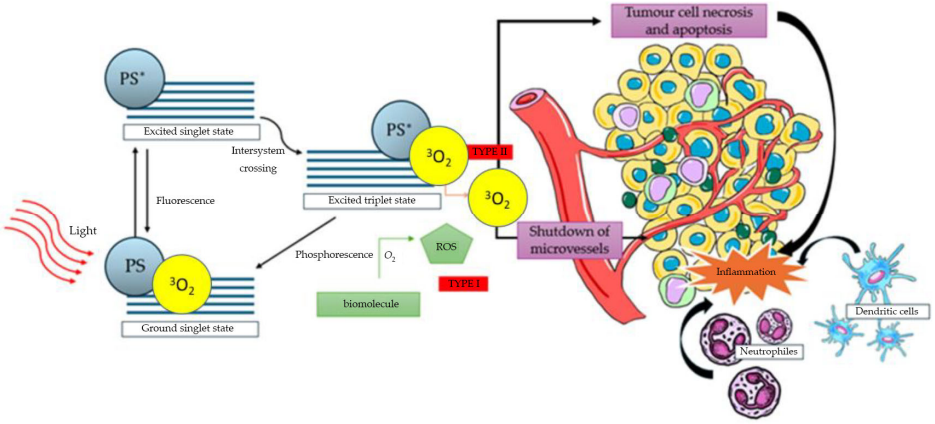


Figure 1. Mechanism of action of PDT demonstrating Type I and Type II reactions in cancer therapy.

Phosphorescence is a competing photophysical process that shows the photosensitizer is in its reactive triplet state, but the real damage comes from the Type I (radical) and Type II (singlet oxygen) chemical reactions that use that triplet state's energy, not the light emission itself. Phosphorescence in PDT is not the primary killer but a brief, energetic intermediate step: a photosensitizer (PS) absorbs light, jumps to an excited singlet state, then quickly converts to a longer-lived excited triplet state (T1) via intersystem crossing (ISC)—this triplet state is the key for both Type I (radical formation) and Type II (singlet oxygen) reactions, leading to cancer cell death, with phosphorescence being light emission from this triplet state, showing it is active but often overwhelmed by the cytotoxic pathways.

There are four processes that show how phosphorescence fits with Type I and II reactions, and these are as follows:

I: Light absorption and singlet state (S1) generation: the PS absorbs light, goes to S1 (excited).
II: Intersystem crossing (ISC): S1 quickly becomes T1 (triplet state)—this is where phosphorescence occurs (PS* $\rightarrow$ PS + light), but it is a minor pathway compared to energy/electron transfer.
III: Type I reaction (radicals): PS(T1) transfers an electron or H-atom to nearby molecules (like O_2 or tissue), creating radicals ($O_2^{-}\bullet$, HO$\bullet$, H_2O_2) that damage cells.

IV: Type II reaction (singlet oxygen): PS(T1) transfers energy directly to ground-state oxygen ($^3O_2$), creating highly toxic singlet oxygen ($^1O_2$), the main killer.

The effectiveness of PDT largely depends on the selection of an appropriate photosensitizer. The ideal PS should be characterized by high purity, the ability to effectively generate singlet oxygen, low toxicity in the dark [28], and the ability to absorb light in the so-called "therapeutic window" (600–800 nm), which allows light to penetrate deep into the tissue [24]. Currently, one of the most commonly used classes of photosensitizers are porphyrin derivatives [29], which, due to their unique photochemical properties, are widely used in both clinical trials and medical practice [30]. 5-ALA is a naturally occurring substrate of the heme biosynthesis pathway that, when added exogenously, results in the predominant accumulation of protoporphyrin IX (PpIX), a photoactivated porphyrin [31]. Exogenously administered 5-ALA is metabolized into protoporphyrin IX. There were concerns that the amount of enzymes in an ex vivo tissue sample might not be sufficient to transform 5-ALA, so we used the active metabolite instead. Rose Bengal (RB) (4,5,6,7-tetrachloro-20,40,50,70-tetraiodofluorescein disodium) is a chemical compound derived from the xanthene family and originally used as a dye by ophthalmologists to image corneal lesions [32]. In tumor samples, PpIX tends to accumulate inside mitochondria, while RB can localize in lysosomes or the plasma membrane. Using both ensures that multiple cellular structures are damaged simultaneously, reducing the chance of tumor cell survival. Both agents generate ROS when activated by light. Their combination can lead to a synergistic increase in cytotoxicity compared to either agent used alone. This synergy allows for lower concentrations of each drug to be used, potentially reducing "dark toxicity" (damage occurring without light) and minimizing side effects. PpIX is typically activated by blue (405 nm) or red light (630 nm), whereas RB is highly sensitive to green light (550–560 nm).

At 410 nm (deep blue/violet), light penetration in biological tissue is very shallow, typically only around 0.3 to 1 mm, primarily affecting the epidermis and superficial dermis due to strong absorption by melanin and hemoglobin; therefore, in a 2 mm thick tissue sample, most of the light would be absorbed within the first millimeter, with minimal light reaching the full depth, especially in pigmented or blood-rich tissues [33].

Cell death in freeze–thawed tissues is typically determined by assessing membrane integrity, mitochondrial function, or biochemical markers of apoptosis and necrosis. Because freezing and thawing often induce physical damage like ice crystal formation, cell death can be immediate (necrosis) or delayed (apoptosis) [34].

The most common method for evaluating immediate cell death is checking if the cell membrane has been ruptured by ice crystals. In the Trypan Blue Exclusion method, the viable cells exclude the dye, while non-viable cells with damaged membranes stain blue [35]. The use of propidium iodide (PI), a fluorescent dye that only enters cells with compromised membranes, makes it a standard for identifying necrotic or late-apoptotic cells via flow cytometry [35]. Lactate Dehydrogenase (LDH) release measures the release of this cytosolic enzyme into the surrounding medium, indicating membrane rupture [35].

Mitochondrial and metabolic function is tested by determining if cells are still metabolically "active" after thawing. Mitochondrial dyes (JC-1) are used to measure mitochondrial membrane potential. A shift from red to green fluorescence indicates a loss of potential, signaling early cell death [36]. Mitochondrial Dehydrogenase activity in assays like MTT or XTT measures the ability of living cells to reduce salts into colored products.

Finally, histological and morphological examination is used for microscopic analysis to reveal "freeze–thaw artifacts" that serve as indirect evidence of cell death [37,38].

Histology after PDT is crucial to assess treatment efficacy by revealing tumor cell death (necrosis), the extent of immune cell infiltration (like T cells, macrophages), and the subsequent

tissue repair/remodeling, confirming if the therapy achieved its goals (destroying cancer, triggering immunity, stabilizing vessels) or needs adjustment. It provides microscopic proof of PDT's complex effects, showing tumor destruction, inflammation, and healing, helping optimize future treatments. Using multiple photosensitizers with different absorption spectra can help overcome the limitations of light penetration in thick or heterogeneous tumor tissues. PpIX is a well-known fluorophore used for fluorescence-guided surgery to visualize tumor margins. RB, which has also been used for diagnostic staining, adds another layer of therapeutic potency through its strong photodynamic and immune-activating properties. This study evaluated the effect of PDT using two photosensitizers—exogenous PpIX and RB—on histopathological changes in NMIBC pTa LG tissues ex vivo. The experiment confirms the postulated thesis that photodynamic therapy is effective in destroying the tissue of non-invasive low-grade urothelial cancer. Moreover, the tested photosensitizers, especially RB, have not been used in PDT for urothelial bladder cancer so far. In our study we searched for physical artifacts before and after PDT to detect expanded extracellular spaces, shrunken cells, and "pseudobubbles" in tissues.

2. Materials and Methods

2.1. NMIBC pTa LG Tissue Samples

Patients with a neoplastic lesion in the urinary bladder underwent a transurethral resection of bladder tumor (TURBT) at the Department of Urology, Clinical Hospital No. 1, Rzeszów, Poland. Tissue fragments recovered after the procedure were transferred to the Department of Pathomorphology at the same hospital. We collected n = 30 samples. All tissue sample measuring 5 × 5 × 2 mm was obtained and frozen in a cryostat Leica CM3050S manufactured by Leica Biosystems (Deer Park, IL, USA) at temperatures below −17 °C and then transported within 10 min to the tissue bank of the University of Rzeszów for storage at −72 °C in 75% Complete Growth Medium + 20% FBS + 5% DMSO. The remaining tissue material was subjected to standard formalin-fixation processing. Then, when a diagnosis of NMIBC was confirmed, the previously acquired tissue sample was selected for analysis. On the day of the experiment, the tissues were thawed to room temperature [39,40] and cut to form two samples—both measuring 5 × 5 × 2 mm. The first sample was immediately placed in a 10% neutral buffered formalin solution and later processed to create a model preparation without PDT effects for comparison. The second was incubated with oxygen-saturated solution of PpIX (1–3 mM) or RB (0.300–0.500 mM) for 1 h in darkness, irradiated with 410 nm or 532 nm laser light (300 mW) for 15 min, and subsequently also processed for hematoxylin–eosin histology examination. This comparative method allowed researchers to avoid overdiagnosis of cellular changes related to the thawing process as effects of PDT. The study was conducted in accordance with the Helsinki Declaration and approved by the Ethics Committee of the University of Rzeszów (protocol code 29/05/2019 and date of approval: 9 May 2019).

2.2. Photosensitizers

The following photosensitizers were used in this experiment: protoporphyrin IX disodium salt (PpIX; Sigma-Aldrich, St. Louis, MO, USA) in 12 samples, at concentrations of 1 mM, 2 mM, and 3 mM; and Rose Bengal disodium salt (RB; 95%, Sigma-Aldrich, St. Louis, MO, USA) in 12 samples, at concentrations of 0.3 mM, 0.4 mM and 0.5 mM. Water purified in an AquaB Duo reverse osmosis system (Fresenius Medical Care, Singapore) was used to prepare the photosensitizer stock solutions. Before application to bladder cancer tissue samples, the solutions were saturated with oxygen (99%, STP; DIN Chemicals, Bielsko-Biala, Poland) for 10 min. The chemical stability of the PS under these conditions was confirmed via UV-Vis spectroscopy, showing no signs of oxidative degradation prior

to light exposure. All samples were used immediately after oxygenation to ensure maximum reproducibility and to prevent gas escape or secondary dark reactions. To avoid aggregation, we monitored the PS state using UV-Vis absorption spectroscopy. Specifically, we looked for the characteristic Soret band broadening and blue-shift (H-aggregates) for PPIX and changes in the absorption peak for RB.

2.3. Photodynamic Protocol

The NMIBC pTa LG tissue samples were individually warmed to room temperature and placed in the center of a plastic Petri dish for the addition of the oxygenated photosensitizer stock solution. Immediately after oxygenation, a volume of 0.1 mL of the respective stock solution was topically spread on the tissue drop by drop, allowing the solution to cover the entire surface of the NMIBC pTa LG tissue sample. The collected samples had a volume of $5 \times 5 \times 2$ mm $\pm$ 1 mm. The photosensitizer-coated tissues were then covered and kept in the dark for 1 h before irradiation. After 1 h in the dark, the Petri dish containing the covered tissue samples was placed under a light source and illuminated for 15 min. The PS solution was removed from the sample. The distance of the light source from the tissue surface was chosen so that the irradiation area was 25 mm^2, and the irradiation of the samples did not cause the tissue to heat up above 30 °C, as measured with a CPR-411 temperature probe (Elmetron, Zabrze, Poland). A CNI Laser (Changchun, China) at 410 nm was used to irradiate the PpIX-treated samples. RB-treated samples were illuminated with a laser at 532 nm. Immediately after 15 min of illumination, the samples were placed in a glass vial containing 10% buffered formalin solution (4% formaldehyde solution) for histopathological evaluation by microscopy. The beam was delivered via a single-mode fiber and was terminated by an adjustable achromatic collimator (PicoQuant). The laser beam was defocused and homogenized using a ground-glass diffuser (Thorlabs, Newton, NJ, USA) and placed immediately above the culture dish to ensure uniform illumination of the entire 5 mm^2 culture area at an average power density of 40 mW/cm^2 (200 mW total power over 25 mm^2). The distance between the collimator output and the cell monolayer was fixed at 20 cm.

Laser fluence was calculated using the formulas: energy [J] = power [W] $\times$ time [s], and fluence = energy [J]/area [cm^2]. For the irradiation of 25 mm^2 cell culture area with 200 mW laser during 15 min (900 s) the fluence was 72 J/cm^2.

2.4. Histopathological Preparations

Histological slides of NMIBC pTa LG tissue specimens were prepared in the Clinical Pathology Department of Clinical Hospital No. 1. A tissue processor (Leica TP1020, Leica Biosystems, Deer Park, IL, USA), paraffin embedder (Leica EG1150H, Leica Biosystems, Deer Park, IL, USA) and coverslip (Leica CV5030, Leica Biosystems, Deer Park, IL, USA) were used. Surgical material for histopathological examination was fixed for 24 h in 10% buffered formalin solution (4% formaldehyde solution). After fixation of NMIBC pTa LG fragments, tissue sections were collected into cassettes. Tissue material from the cassettes was washed, dehydrated, passed through intermediate fluids and embedded in paraffin to obtain blocks. The sections were stained with hematoxylin and eosin. A universal histopathology slide-staining device (LEICA ST 5020 Multistainer, Leica Biosystems, Deer Park, IL, USA) was used for this purpose. The final step was to cover the scrapings with a coverslip; the space between the coverslips was filled with histologic fluid.

2.5. Microscope Examination

Histological examinations of the tissues used in the study were performed at the Pathology Department of the Clinical Hospital No. 1 in Rzeszów. Histological image analysis was performed using a Leica DM1000 LED microscope (LEICA Microsystems,

Wetzlar, Germany). The extent of NMIBC pTa LG tumor cell damage after PDT was assessed based on histological features and immunohistochemical staining. Absence or improper shape of papillary structures (a characteristic architectural feature of noninvasive papillary urothelial carcinoma low-grade) or irregular layering of epithelial cells was recognized as an architectural disorder. At higher magnification, the intensity of hematoxylin staining of the cell nucleus (the degree of hyperchromasia), presence of irregular nuclear contours, and the eventual presence and extent of nuclear chromatin "blots" resulting from damage and fusion of the nuclei of adjacent cells after disruption of the cell membranes were identified. The mentioned qualitative assessment has proven reliable in another PDT experiment performed by the authors [41]. In addition samples underwent immunohistochemical staining for cleaved caspase-3 to detect and quantify apoptotic cells.

Tissue damage associated solely with the freezing process is significantly less severe. Comparing histopathological slides prepared from frozen sections without therapy to those frozen and treated with PDT allows us to assess the effectiveness of the treatment.

Histological and morphological examination was performed by microscopic analysis to reveal "freeze–thaw artifacts" that serve as indirect evidence of cell death. We searched for physical artifacts to detect common findings including expanded extracellular spaces, shrunken cells, and "pseudobubbles" in tissues. We detected that karyopyknosis means deeply stained, shrunken nuclei, often visible in formerly frozen tissues. However, the number of abnormal cells in material before PDT was less than 15%.

The study was conducted on tissue collected from "real" patients with non-invasive, low-grade urothelial carcinoma, whose tumors must have exhibited various combinations of mutations. The physical damage from freezing alters how photosensitizers distribute within the tissue, meaning any observations regarding localization or uptake do not reflect "real-patient" or in vivo conditions. The proportion of possibly damaged cells was less than 15%, confirmed by histopathology. In the authors' opinion, it complements studies performed on pre-existing cell lines, which are clones of the same cell with the same set of mutations. Tissue damage during the freezing process in a cryostat causes only minor morphological changes. This technique is commonly used for intraoperative examinations and allows for the reliable assessment of, for example, a specific type of cancer. A section of each tissue sample was subjected to the freezing process without PDT and served as a reference point for assessing treatment outcomes. The purpose of cryopreserving tissues is to help prevent ice crystal formation in tissue when water freezes and expands. Ice crystals break cell membranes and produce holes within cells and loose extracellular matrix (Swiss Cheese artifacts). The two basic strategies for preventing crystals during the transition from water to ice are: (1) freeze as rapidly as possible and (2) add cryoprotectants that disrupt interaction between polar water molecules. Cryoprotectants are particularly important when freezing large tissue samples. The changes in the tissues after PDT were significantly more severe than those present in the reference sections. This assessment method has already been successfully used in other experiments [42].

2.6. ROS Measurements

The quantitative ROS measurements were generated by performing Singlet Oxygen Generation assay by using 1,3-Diphenylisobenzofuran (DPBF).

DPBF assay is a chemical trapping method used to determine the singlet oxygen quantum yield in organic solvents or aqueous solutions. DPBF was dissolved in a suitable solvent DMSO to a concentration of 1.0 mM. The solution was stored in the dark as it is highly light-sensitive. The solution of standard reference Rose Bengal in water is $\Phi = 0.75$. PS and DPBF were mixed in the solutions in a cuvette. The typical working concentration

for DPBF was 20 µM. The PS concentration was set so that the initial absorbance at the excitation wavelength was low (typically <0.1) to avoid inner filter effects.

2.7. MRI Measurements

In regard to viability measurements, since we used tissue ex vivo we performed MRI. A decrease in contrast enhancement within 2 to 24 h after PDT strongly correlates with the successful reduction in tissue viability.

For 1.5T MRI evaluating post-PDT shutdown, a T1-weighted gradient echo sequence with 3.5–5.0 ms TR, 12–15° flip angle, and a temporal resolution under 10 s was recommended. Investigations were performed using a 1.5 Tesla MR system. A dedicated surface coil or a phased-array body coil was used to ensure high signal-to-noise ratio (SNR) over the treated area. The tissue samples were immobilized to minimize motion artifacts, which is critical during dynamic acquisition. T1-mapping was performed to calculate the baseline longitudinal relaxation time. Regions of Interest (ROIs) are drawn around the PDT-treated zone and adjacent healthy tissue [43].

3. Results

3.1. Effect of PpIX-PDT on Morphology of NMIBC pTa LGs

Before PDT, distinguishing between artifactual damage and true biological cell death requires careful interpretation. In freeze–thawed tissues, cell death is determined by identifying specific morphological artifacts because freezing creates significant structural artifacts (e.g., ice crystal clefts). We used morphological indicators (Light Microscopy) and standard H&E (hematoxylin and eosin) staining to reveal structural changes that indicate irreversible cell damage or death before PDT. We did not see large "clefts" or gaps between cells which are often artifacts of ice crystal formation rather than biological edema, but did notice some single changes.

Figures 2–4 present the effects of PpIX-PDT on the morphology of NMIBC pTa LGs.

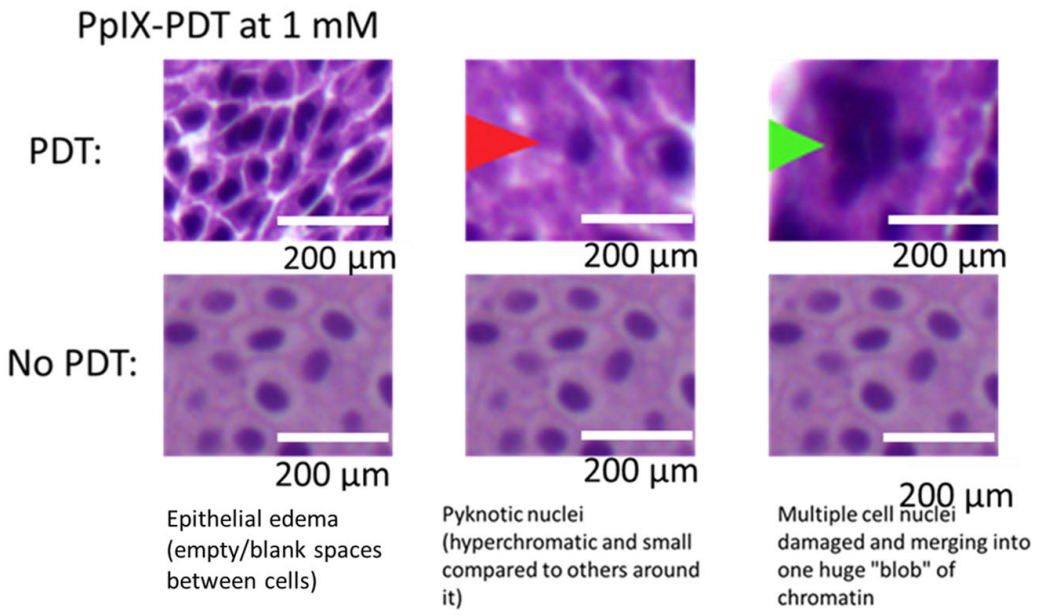


Figure 2. Histological changes in NMIBC pTa LG tissue before and after PpIX-PDT at 1 mM photosensitizer concentrations. Arrows: red—pyknotic nuclei; and green—chromatin condensation.

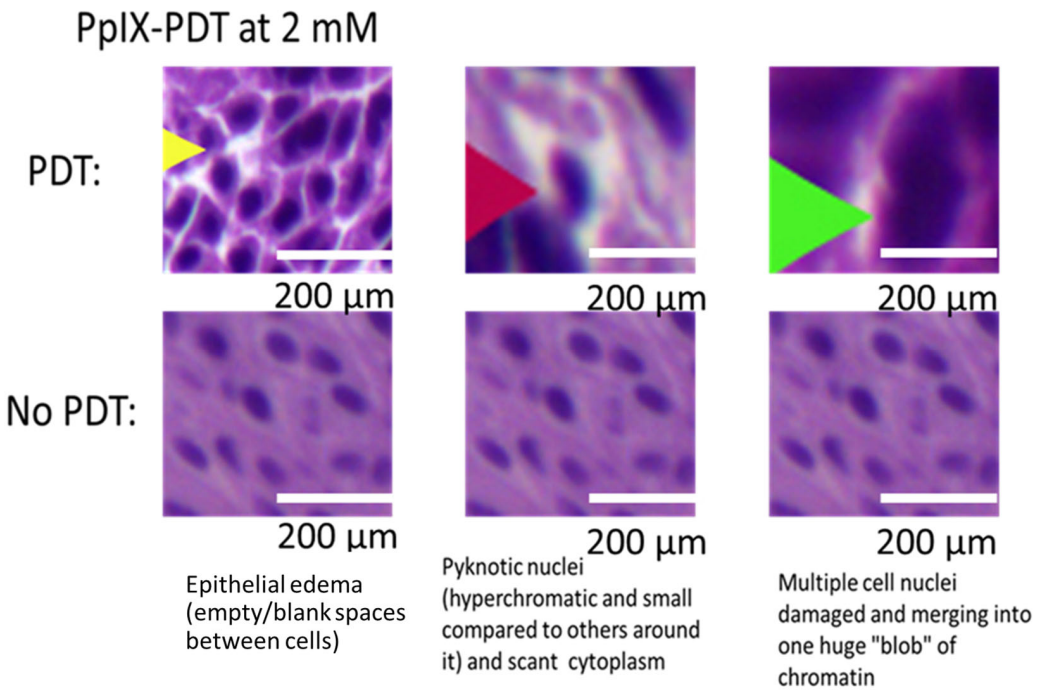


Figure 3. Histological changes in NMIBC pTa LG tissue before and after PpIX-PDT at 2 mM photosensitizer concentrations. Arrows: red—pyknotic nuclei; yellow—epithelial edema; and green—chromatin condensation.

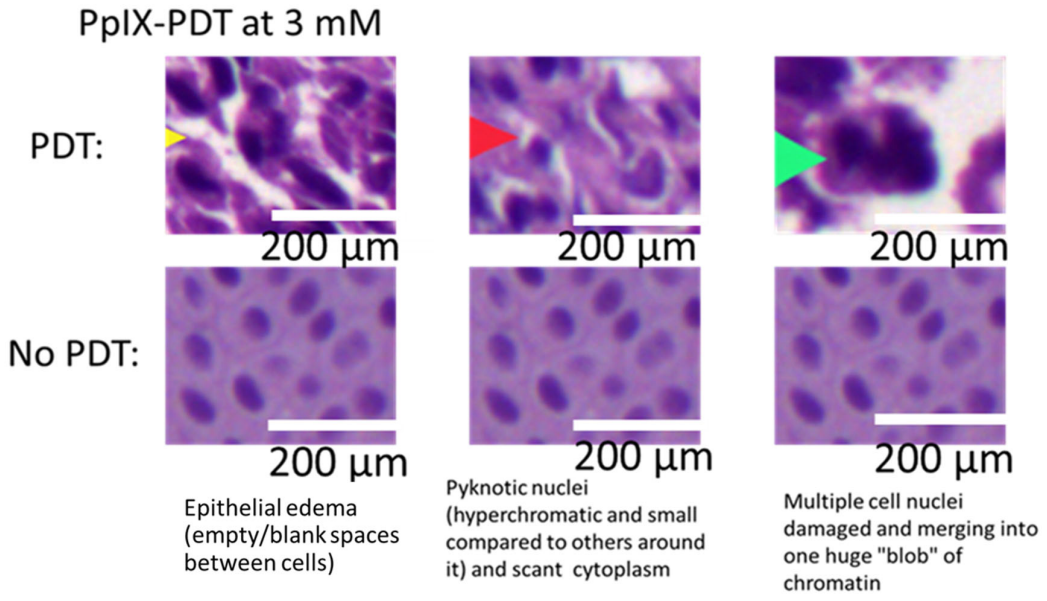


Figure 4. Histological changes in NMIBC pTa LG tissue before and after PpIX-PDT at 3 mM photosensitizer concentrations. Arrows: red—pyknotic nuclei; yellow—epithelial edema; and green—chromatin condensation.

Even at a concentration of 1 mM, edema of the stroma, and initial architectural abnormalities, mainly irregular layering of epithelial cells, were identified; at 200× magnification moderate chromatin condensation was observed in the vast majority of cell nuclei. The number of pyknotic cells was moderate. Increasing the concentration to 2 mM resulted in more pronounced nuclei chromatin condensation and pyknosis, the forming of a few chromatin "blots" along with the disruption of tissue organization. The strongest effects were seen at 3 mM—at 100× magnification extensive and severe structural damage can be detected, while at 200× magnification pronounced chromatin condensation, numerous pyknotic nu-

clei and a higher number of chromatin "blots" were evident. Such concentration-dependent potentiation of phototoxic effects unequivocally confirms the effectiveness of PpIX-PDT in inducing morphological damage to NMIBC pTa LG cells.

According to the study's protocol, the use of oxygen-saturated PpIX serves a specific biochemical purpose distinct from standard clinical photodynamic therapy goals, particularly when considering tissue damage caused by the freeze–thaw process.

After PDT an analysis of cells indicated dead cells. Dead cells often fail to regain their original volume after thawing due to osmotic stress, appearing shrunken with dark, condensed nuclei (pyknosis). Dead cells typically exhibit increased eosinophilic (pink/red) staining, appearing "glassy" or more intense than viable cells. High-magnification examination may reveal ruptured plasma membranes or ruptured lysosomes, which cause the tissue to appear "mushy" or liquefied. The permanent loss of cell-to-cell connections that do not redevelop upon thawing is a primary indicator of tissue-level death.

3.2. Effect of RB-PDT on Morphology of NMIBC pTa LGs

Figures 5 and 6 present the effects of RB-PDT on morphology of NMIBC pTa LGs.

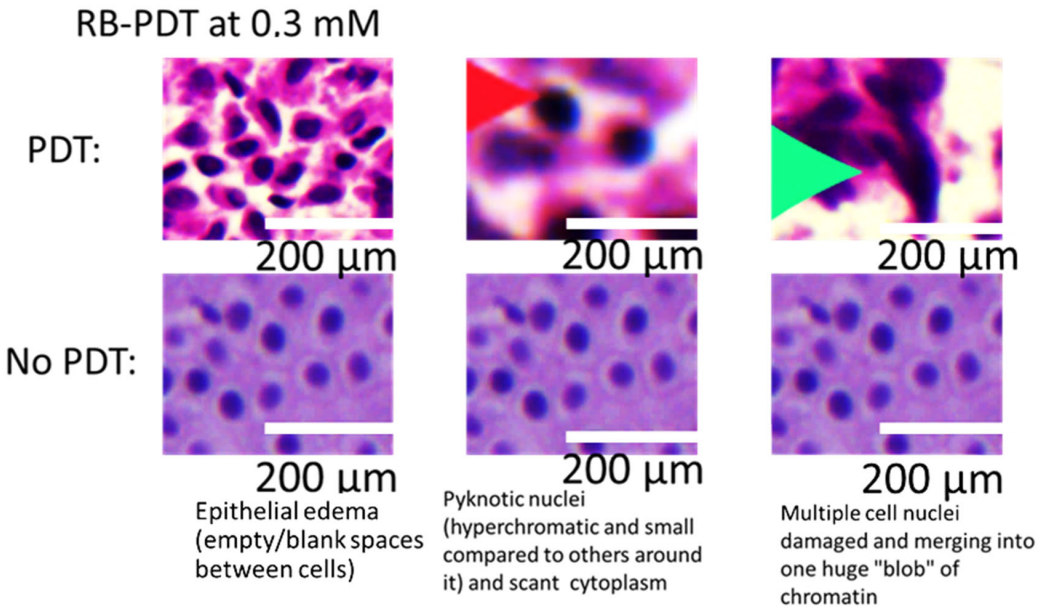


Figure 5. Histological changes in NMIBC pTa LG tissue before and after RB-PDT at 0.3 mM photosensitizer concentrations. Arrows: red—pyknotic nuclei; and green—chromatin condensation.

At a concentration of 0.3 mM, discrete-to-moderate chromatin condensation is evident in most cell nuclei, and the presence of pyknotic nuclei, swollen stroma and blurred intercellular boundaries were noted, with almost unchanged tissue architecture. The 0.4 mM concentration tissue sample revealed the presence of thrombotic necrosis, which made the evaluation of the effects of PDT impossible. In contrast, at the highest concentration of 0.5 mM, mild-to-extensive chromatin condensation, numerous pyknotic nuclei and swelling of the stroma, as well as significant structural abnormalities of the tissue architecture were observed. The described changes clearly indicate a concentration-dependent potentiation of the phototoxic effects of RB-PDT.

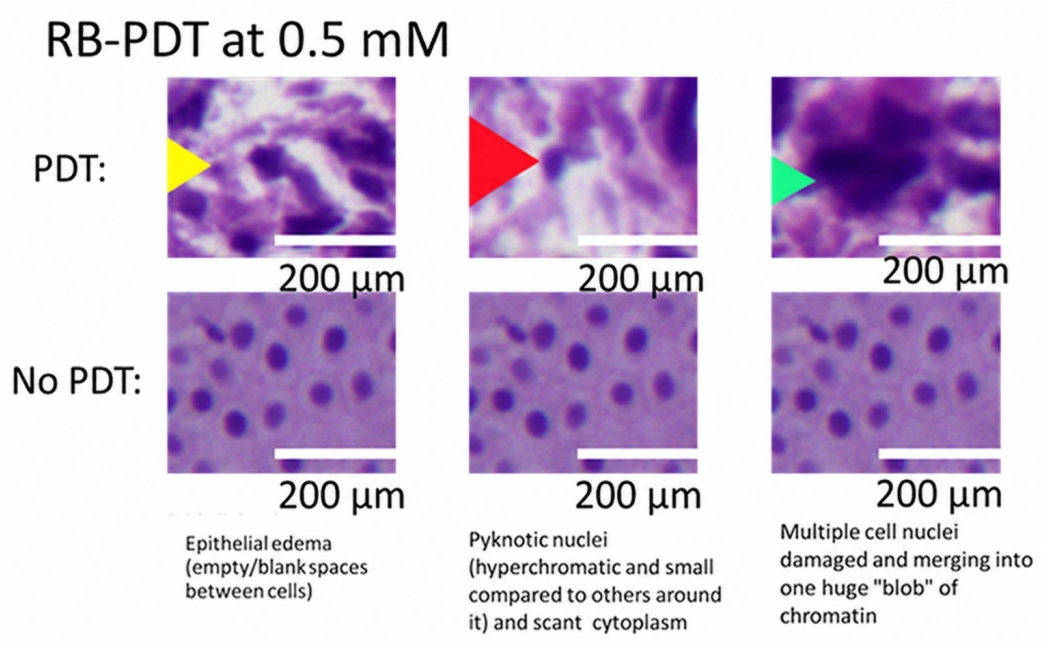


Figure 6. Histological changes in NMIBC pTa LG tissue before and after RB-PDT at 0.5 mM photosensitizer concentrations. Arrows: red—pyknotic nuclei; yellow—epithelial edema; and green—chromatin condensation.

3.3. Cells with Pyknotic Nuclei in the Fields of View After PpIX-PDT and RB-PDT

To evaluate the effects of PDT (Tables 1 and 2), five large fields of view were selected from random, representative locations within each slide. Pyknotic cells (undergoing apoptosis) that had a positive caspase-3 IHC stain reaction were identified within each field and their number per 100 cancer cells was calculated. Results presented in Tables 1 and 2 (as percentages) show the correlation between the concentration of the photosensitizers used and the number of identified pyknotic cells. The detected number of apoptotic cells in the control samples without PDT treatment may be related to the aftermath of the tissue freezing process.

Table 1. Number of cells with pyknotic nuclei in the fields of view after PpIX-PDT.

	Field 1	**Field 2**	**Field 3**	**Field 4**	**Field 5**	
Concentration Pp IX [mM]						**Average Quantity**
No PDT	3%	4%	4%	3%	5%	3.8%
1 mM	14%	12%	9%	18%	16%	13.8%
2 mM	22%	23%	19%	31%	24%	23.8%
3 mM	43%	41%	37%	45%	39%	41.0%

Table 2. Number of cells with pyknotic nuclei in the fields of view after RB-PDT.

	Field 1	**Field 2**	**Field 3**	**Field 4**	**Field 5**	
Concentration RB [mM]						**Average Quantity**
No PDT	2%	5%	5%	6%	2%	3.9%
0.3 mM	17%	19%	22%	17%	19%	18.8%
0.5 mM	37%	36%	34%	29%	41%	35.4%

One pathologist carried out the examination; he was blinded to the samples.

In necrotic tissue, the cell membrane is damaged, and cytoplasmic contents leak out. They form an amorphous, acidophilic mass. Cells may be enlarged ("swollen") and vacuolated. Karyolysis and karyorrhexis of cell nuclei are present. Some of the dissolved nuclei blend together. A pyknotic nucleus in an apoptotic cell is smaller in size, round or oval and the cell membrane is usually intact. The typical architecture of a noninvasive papillary urothelial carcinoma low-grade consists of neoplastic urothelium formed by cells that are uniform in size, have no significant nuclear pleomorphism but may have occasional slight irregularities in nuclear contour lining fibrovascular cores. There is only minimal fusing or branching of the papillae. Cell membranes (intercellular "borders") are identifiable. Cells with blurred borders; confluent cytoplasm; enlarged, irregular, confluent, hyperchromatic nuclei; and those without identifiable typical structures such as the nuclear membrane or nucleolus were considered damaged.

A lack of layered arrangement to the epithelial cells, the separation of epithelial cells from the stroma or from each other, and the effacement/disruption of the papillary structures were considered architectural abnormalities. It reveals if PDT caused only superficial damage (ideal for superficial tumors) or deeper necrosis, helping to adjust light doses to spare healthy tissue. It is essential for spotting tiny, flat lesions or viable tumor remnants that might be missed during imaging or cystoscopy, preventing recurrence.

In the context of the described protocol, using oxygen-saturated protoporphyrin IX (PpIX) likely serves as an internal standard or a reporter of cellular oxygenation. During the photodynamic reaction, the excited photosensitizer transfers energy to ground-state molecular oxygen to create cytotoxic singlet oxygen. This process can consume oxygen at rates as high as 6–9 microM/s. When the rate of oxygen consumption exceeds the rate of diffusion from the surrounding environment, local oxygen levels drop rapidly, which can bring ROS production—and thus the therapy's effectiveness—to a halt [44,45]. PpIX delayed fluorescence is a known technique for measuring mitochondrial oxygen tension (mitoPO2). By saturating the sample with oxygen, researchers can establish a "baseline" or maximum potential for the photodynamic reaction, which is inherently oxygen-dependent. Because solid tumors (and potentially those frozen in cryostat tissues) often suffer from hypoxia, which limits PDT efficacy, saturating with oxygen ensures that the observed cytotoxicity is a result of light/photosensitizer interaction rather than being limited by oxygen availability. When the supernatant is present, the photosensitizer remains in close proximity to the outer cell membrane. Light activation then generates reactive oxygen species (ROS) in the immediate extracellular environment, leading to rapid membrane disruption, lipid peroxidation, and protein crosslinking. This bypasses the selective uptake process typically required for clinical PDT, where the sensitizer should accumulate inside the cell (e.g., in mitochondria or lysosomes) to trigger targeted apoptosis. Irradiating with the supernatant can cause cells to become distorted, round, or detached from culture plates more aggressively than if the sensitizer were only intracellular.

When PDT is carried out in vivo, enough time elapses so that all of the photosensitizer is internal. This will cause photodamage to sub-cellular loci where the photosensitizer is concentrated: often mitochondria for the most effective agents. Mitochondrial damage results in the release of cytochrome c into the nucleus, a trigger for apoptosis. Irradiation triggers the production of reactive oxygen species (ROS) directly at mitochondrial membranes. This localized oxidative stress causes the permeabilization of the mitochondrial outer membrane and the opening of the mitochondrial permeability transition pore. Consequently, cytochrome c is released from the mitochondrial intermembrane space into the cytosol. Once in the cytosol, cytochrome c forms the apoptosome complex, which activates caspase-9 and subsequently caspase-3, initiating the programmed cell death (apoptosis)

pathway. Freezing and thawing tissue prior to experiments induces mechanical disruption of cell membranes and organelle structures. This compromises the integrity of the mitochondria and other sub-cellular loci, likely leading to necrosis rather than controlled apoptosis. By irradiating without washing away the extracellular photosensitizer, the light acts on the outer cell membrane and the extracellular matrix first. This causes rapid, non-specific membrane destruction and prevents the selective mitochondrial damage that characterizes effective in vivo treatment. Consequently, the results obtained from this experimental setup reflect a non-physiological cytotoxic event (primarily necrosis and membrane rupture) rather than the precise, mitochondria-mediated apoptotic mechanism seen in clinical PDT. Both PpIX and RB photosensitizers demonstrated a clear dose-dependent relationship with cellular damage.

During PpIX-PDT experiments, increasing the concentration from 1 mM to 3 mM resulted in a significant rise in pyknotic (apoptotic) cells, peaking at an average of 41.0%.

During RB-PDT experiments, Rose Bengal showed high potency at lower concentrations compared to PpIX; a concentration of only 0.5 mM RB yielded 35.4% pyknotic cells, nearly matching the effect of 2–3 mM PpIX.

3.4. The Quantitative ROS Measurements

The initial absorbance of DPBF at 410–415 nm was registered. The sample was irradiated using a light source in timed intervals (e.g., every 15–30 s). The decrease in DPBF absorbance after each interval was observed. The rate of degradation is proportional to the amount of singlet oxygen generated.

3.5. The Quantitative MRI Measurements

The untargeted tissue (before PDT) typically shows longer T1. After PDT treatment a "black-out" effect is observed in the treated area. After PDT, the lack of signal enhancement indicates tissue shutdown. There is a statistically significant decrease in values (often >50% reduction) compared to untreated samples. T1 values were measured for healthy bladder tissue, NMIBC tissue and NMIBC tissue after RB_PDT and Exogenous PpIX-PDT. The mean T1 time in the healthy tissue was 1351.7 $\pm$ 271.1 ms, while a significantly shorter relaxation time (727.7 $\pm$ 145.0 ms) was recorded in the NMIBC group, and this was further reduced to 504 $\pm$ 11 ms after RB-PDT and 567.3 $\pm$ 8. Analysis of variance (ANOVA) showed a very strong significance of differences between groups ($F = 184.4$; $p < 0.0001$), and post hoc tests confirmed that all comparisons (healthy vs. NMIBC, healthy vs. NMIBC_PDT, NMIBC vs. NMIBC_PDT) were statistically significant at the $p < 0.001$ level.

4. Discussion

In our experiments, we showed that both PpIX-PDT and RB-PDT induce morphological changes in NMIBC pTa LG tissue that are primarily characteristic of apoptosis—such as chromatin condensation, pyknosis and nucleus fragmentation [46,47].

For PpIX-PDT, a concentration-dependent severity of effects was observed: from discrete chromatin condensation and mild architectural abnormalities at 1 mM to pronounced hyperchromatic nuclei and features of advanced cell damage at 2 mM, and massive chromatin condensation with extensive structural damage at 3 mM. Similarly, RB-PDT showed discrete-to-moderate chromatin condensation and minor architectural abnormalities at 0.3 mM, no diagnostic reading due to thrombotic necrosis at 0.4 mM, and mild-to-extensive chromatin condensation and significant structural damage at 0.5 mM. Overall, Rose Bengal induced more intense and faster cytotoxic effects, likely due to its better retention in cells and the efficient generation of singlet oxygen; fluorescence microscopy could help clarify this issue.

The process of freezing and thawing itself can induce independent ROS generation (oxidative stress), which would contaminate data and make it impossible to distinguish between ROS caused by the PDT treatment and ROS caused by the cryopreservation process. In laboratory settings (in vitro), cell viability for specific cancer lines often remains above 85% when treated with therapeutic concentrations of photosensitizers before laser activation. Significant cell death only occurs once light is applied.

Low oxygen levels in tumor tissue severely hinder the efficiency of Type II PDT reactions, which require oxygen to produce the cytotoxic singlet oxygen needed to kill cells. Thus, we used oxygen-saturated solutions PpIX and oxygen-saturated solutions of RB.

Herein, we summarize (Table 3) the relevance of the new material relating to the freezing of cells.

Table 3. The features of PDT in fresh cells vs. PDT in frozen cells.

Feature	PDT in Fresh Cells	PDT in Frozen (Cryopreserved) Cells
Viability	>99% before treatment; high activity.	~85% or lower; cells are stressed.
ROS Baseline	Natural; low background noise.	Elevated due to freeze–thaw cycles.
Membrane State	Intact; perfect for testing surface ablation.	Potentially compromised by ice crystals.
Goal in Study	To perform the treatment.	To preserve the result for microscopy.

Studies using freeze–thawed tissues to evaluate the effectiveness of photosensitizers like PpIX and RB are often criticized for their clinical relevance. These samples lack critical factors found in live tissues, such as metabolic activity, intact cell membranes, and oxygenated microenvironments, which are essential for real-world PDT efficacy. Many cells in freeze–thawed samples do not burst immediately but instead activate stress-response pathways. This leads to Cryopreservation-Induced Delayed-Onset Cell Death (CIDOCD), which is predominantly apoptotic and peaks 6–24 h post-thaw [48]. The rapid freezing process allows for "freezing time" in the sample. In living tissue, metabolic processes, including photosensitizer degradation or changes in oxygen concentration, occur dynamically, which can lead to inconsistent results. Freezing ensures the morphological and molecular stability of the tested material. Working with frozen sections allows for multiple series of measurements on identical material under controlled laboratory conditions. This eliminates variability resulting from factors such as blood flow (perfusion) or tissue oxygenation in a living patient, facilitating the isolation of specific physicochemical parameters of the photodynamic reaction. Using material from biobanks or samples collected previously (e.g., during a biopsy) is often the only option for preliminary research. According to regulations on medical experiments, research on biological material already collected (e.g., frozen) is permissible and often constitutes a precursor to clinical trials on living tissue. In cryosections, it is easier to precisely assess the depth of light penetration and the distribution of the photosensitizer in individual tissue layers using fluorescence microscopy, which is technically much more difficult to map in vivo (living) tissues. PDT generates heat that can damage tissue. Studies on frozen materials allow us to model the effect of temperature on the quantum yield of reactive oxygen species generation without the risk of inflicting pain on the test subject. Freezing and thawing affect endogenous fluorophores such as NAD(P)H and flavins. Frozen tissues exhibit smaller and delayed metabolic changes in response to activation compared to fresh tissues, paradoxically allowing for the study of the "baseline state" of the tissue without the disruption of a sudden reaction to external stimuli. When arguing for the choice of frozen tissues, it is worth emphasizing that although they differ from in vivo tissues, they constitute a more predictable and reproducible research model for calibrating optical systems and assessing the distribution of photosensitizers. Cryosections

are usually thicker than paraffin sections, which may result in lower microscopic resolution and less precision in reproducing morphological details. It is actually relatively easy to freeze cells and recover them. It is harder to freeze tissues and have them come back. Cell lines are routinely frozen and stored for decades. The American Type Culture Collection (ATCC) has some guidelines and explains. Most cell cultures can be stored for many years, if not indefinitely, using cryopreservation. Tissues are harder (though not necessarily impossible) because the structure is easily disrupted and because it is harder to evenly freeze the cells that are part of it. The smaller the tissue, the better the chance of successful freeze and recovery. Tissues are frozen when they are very tiny—at an early-enough stage (100 cells or fewer) that they can be readily permeated by cryoprotectants. PDT relies on the interaction between a photosensitizer, light, and molecular oxygen present in the tissue. Freezing significantly impacts levels of metabolites and essential antioxidants like glutathione (GS) and ascorbate, which can skew the biochemical response to therapy.

Below we present a summary (Table 4) regarding the methods used to detect dead cells in the tissue.

Table 4. Summary of common methods [34–38].

Method	Target	Indicator of Death
Trypan Blue [34]	Plasma Membrane	Positive (blue) staining
Caspase-3 Assay [35]	Proteolytic Enzymes	Elevated enzyme activity
JC-1 Dye [36]	Mitochondria	Red-to-green fluorescence shift
TUNEL [37]	DNA	Fragmented DNA presence
H&E Histology [38]	Overall Structure	Cell shrinkage, expanded extracellular space

In PDT studies, by utilizing 410 nm (blue) and 532 nm (green) light, the "proof-of-concept" established is that specific photosensitizers can be activated to induce high-efficiency cell killing in vitro, even if these wavelengths have poor penetration for standard in vivo clinical use. The studies proved that 410 nm and 532 nm light are highly effective at activating photosensitizers like PpIX or hematoporphyrin derivatives, often resulting in greater cytotoxic efficiency than the standard clinical 630 nm (red) light because of the higher absorption coefficients at these shorter wavelengths.

Research using 532 nm light established that cell death can occur via photothermal pathways (heat-induced damage) rather than just traditional photodynamic (reactive oxygen species) processes, particularly when using pulsed laser irradiation. The results provided a safety proof-of-concept, demonstrating that blue light (410–418 nm) can inhibit tumor cell growth (e.g., melanoma) without causing significant DNA damage or photoaging in surrounding healthy tissue. While unsuitable for deep-seated tumors, the research established these wavelengths as viable for superficial applications such as early-stage oral cancer, precancerous lesions, or dermatology (e.g., acne or port-wine stains) where deep penetration is not required [32,49,50].

Oxygen from a solution (such as blood plasma or an external irrigation fluid) penetrates tissues primarily through simple passive diffusion driven by a concentration (partial pressure) gradient. Oxygen moves spontaneously from areas of higher partial pressure in the solution to areas of lower partial pressure in the tissues, where it is constantly consumed by mitochondria. The rate of penetration is influenced by Fick's Law, meaning it increases with a larger surface area and a steeper pressure gradient, but decreases as the distance (e.g., due to tissue edema) increases. Relating the results of the present study to reports by other authors faces significant difficulties, although 5-ALA-PDT and HAL-PDT have been widely used in bladder cancer therapy studies [51]. In clinical settings, exogenous proto-

porphyrin IX (PpIX) is not administered directly. Instead, it is produced as an endogenous byproduct of the metabolism of its administered precursor, 5-ALA. Traditional clinical PDT (using Photofrin) often causes permanent bladder contraction and muscle damage because it penetrates too deeply. This protocol uses RB and green light (532 nm), which have a shorter penetration depth, specifically to spare the underlying muscle layer while destroying superficial (pTa) tumors. PpIX is already FDA-approved for photodynamic diagnosis (PDD) of bladder cancer because it naturally accumulates 17 times more in urothelial tumor cells than in healthy tissue. Using it for PDT leverages this existing, proven high selectivity.

While some experimental studies have investigated direct application of exogenous PpIX or its esters, standard clinical practice relies on the administration of ALA to induce PpIX accumulation in target tissues. The results obtained in our work correlate with observations from experiments conducted on mouse models of urothelial carcinoma, in which Arum et al. demonstrated induction of apoptosis after HAL-PDT, confirmed by a significant increase in caspase-3 activity [52], while Grönlund-Pakkanen et al. noted that 5-ALA-PDT leads to massive necrosis of tumor cells [53]. A comparison with the effects obtained with RB in the treatment of bladder cancer is not possible, since, to the best of our knowledge, no clinical or preclinical studies using this photosensitizer in the treatment of this disease have been described to date.

Both photosensitizers studied show a similar mechanism of action. PpIX consists of a porphyrin ring with a pronounced hydrophobic character, flanked by two carboxyl groups, which give it amphiphilic properties—it dissolves in the aqueous phase, while tending to penetrate the hydrophobic core of the lipid bilayer, stabilizing at the interface between lipid heads and fatty acid chains [54]. Consequently, PpIX accumulates primarily in the cell membrane [55,56]. On the other hand, the disodium salt of RB, characterized by high water solubility and significant negative charge [57], does not passively penetrate the lipid bilayer due to its high molecular weight. Therefore, it accumulates mainly on the outer surface of the cell membrane or in the surface layer of tissues, while its intracellular transport requires the participation of specific OATP transporters [58]. Photosensitizers deposited at the plasma membrane are activated by light, leading to the local generation of ROS directly at the lipid bilayer. The resulting radicals initiate lipid peroxidation and destabilization of the membrane structure, resulting in the loss of integrity, disruption of ionic homeostasis and, ultimately, cell death [59].

The clinical use of 5-ALA-PDT, which involves the generation of PpIX in situ, resulted in NMIBC pTa LG patients refractory to previous intravesical chemotherapies and double BCG therapy achieving complete remission in 78% of patients at three-month evaluation, with 22% remaining disease-free for nearly three years with a low rate of serious complications [9]. The efficacy of exogenous PpIX delivery differs significantly from that achieved via 5-ALA—in vitro, 5-ALA has been shown to have higher selectivity against cancer cells compared to exogenous PpIX, while intravenous administration of exogenous PpIX does not lead to its effective accumulation in cancer cells [60]. Although some gel formulations of PpIX showed some selectivity for accumulation in tumor tissue, this still remained lower than that observed with 5-ALA [61]. Moreover, exogenously administered PpIX also exhibited lower cytotoxicity compared to PpIX endogenously synthesized from 5-ALA, due to the different intracellular localization of these forms. Exogenous PpIX accumulates mainly in the plasma membrane, while PpIX formed from 5-ALA localizes primarily in the mitochondria. Since mitochondria are more sensitive to photodynamically induced damage than the cell membrane, this results in a stronger cytotoxic effect for PpIX produced from 5-ALA, despite similar $^1O_2$ generation [32]. RB has not yet been the subject of clinical trials as a photosensitizer for bladder cancer therapy.

The administration of exogenous protoporphyrin IX (PpIX) for clinical use, primarily in PDT, is shifting toward more targeted and less invasive delivery systems to overcome its natural hydrophobicity and to improve tissue penetration. Beyond standard oral and topical routes, clinicians are expanding into sublingual delivery, instillation, inhalation for bronchial treatments, and intravascular injection. Sublingual delivery of PS is an emerging administration route for PDT and photodiagnosis, particularly for treating oral and laryngeal lesions. This method utilizes the highly vascularized sublingual mucosa to achieve rapid systemic absorption, bypassing the first-pass metabolism of the liver and enzymatic degradation in the gastrointestinal tract [62]. New amphiphilic PpIX derivatives are being developed to prevent the aggregation-induced quenching that typically reduces treatment efficacy in aqueous physiological environments.

Although ex vivo studies provide valuable information on the mechanisms of action of photosensitizers, this experiment used only isolated tissues subjected to a freezing and thawing procedure. Such a model does not fully reflect in vivo conditions, such as the complex architecture of vascularization, the presence of the immune system or the specific tumor microenvironment, which is crucial in terms of the modulation of the tumor microenvironment and activation of the immune response by PDT [63] and the vascular effects it induces [62]. In addition, the lack of a control group, including photosensitizer-treated samples not subjected to irradiation, makes it difficult to clearly separate the effects of the photosensitizer itself from those associated with the preparation procedure and light exposure. In the next stages of research, it is recommended to implement three-dimensional culture models, such as spheroids or bioreactor systems, which more faithfully reflect the structure and microenvironment of the tumor. Subsequently, in vivo studies on animal models are needed to assess the efficacy and safety of PDT in the context of the whole organism, with a particular focus on interactions with the immune system and vascular effects. In parallel, meticulous optimization of therapy parameters—including the selection of photosensitizer dosage and incubation time—should be carried out to achieve maximum therapeutic efficacy with minimal toxicity to healthy tissues. Smaller particles, particularly those in the nanometer range (e.g., 200 nm), are internalized more rapidly through endocytosis or phagocytosis. Research shows that neutrally charged nanoparticles often peak in cellular accumulation within a single hour. The charge of the PS particles significantly influences absorption. Positively charged particles typically permeate cell membranes more easily than neutral or negatively charged ones, leading to faster accumulation.

Samples likely absorbed PSs over an hour due to the material's porous network structure, hydrophilic/adsorptive properties, and the driving forces of diffusion/osmosis, allowing for gradual penetration and trapping within fibers or matrices, with smaller particle sizes or higher surface areas generally leading to faster uptake, creating a significant concentration gradient over time. If the sample material is hydrophilic, it attracts polar molecules (like water carrying the PSs), and the PSs themselves might have surface properties that promote binding (adsorption) to the sample's material. The PSs move from an area of high concentration (the surrounding liquid) to an area of low concentration (inside the sample) until equilibrium is reached, a process that takes time. Smaller PS particles (like microplastics) can penetrate deeper into the material's network more easily than larger ones, and a larger total surface area of the sample promotes quicker interaction.

The study demonstrates that both exogenously administered PpIX and RB in combination with irradiation induce apoptosis-specific morphological changes in NMIBC pTa LG tissue, such as chromatin condensation and pyknosis, with RB inducing stronger and faster cytotoxic effects than PpIX. The concentration-dependent severity of these changes and structural damage confirms the effectiveness of both photosensitizers in inducing

phototoxicity, but differences in the mode of accumulation (cell membrane for PpIX vs. tissue surface layers for RB) may determine their different action profiles. Despite the ability of exogenous PpIX to induce apoptosis in NMIBC cells, its limited selectivity of accumulation against tumor cells [60,64] indicates that it does not meet the criteria for an optimal photosensitizer [65]. RB, on the other hand, although it has not yet been studied in the treatment of bladder cancer, shows promising potential as a photosensitizer for PDT of this cancer. Our results complement previous reports on PDT with PpIX precursors (5-ALA, HAL), providing unique data on direct administration of exogenous PpIX and comparing its efficacy with RB. To translate these observations into clinical applications, further studies using 3D models and in vivo experiments are needed, as well as optimization of therapeutic parameters, including the dosage and incubation time of photosensitizers. Rose Bengal (RB) exhibited superior cellular retention compared to PPIX, which can be attributed to its amphiphilic nature and specific anionic character. Unlike the highly hydrophobic PPIX, which tends to aggregate or associate primarily with lipid membranes, the xanthene structure of RB allows for a more balanced distribution between aqueous and lipid phases. Furthermore, RB is known to target and accumulate effectively within the lysosomes and mitochondria via endocytic pathways. Once internalized, its high affinity for cytoplasmic proteins (such as albumin or glutathione S-transferases) likely creates a reservoir effect, reducing the rate of passive efflux and leading to the prolonged retention observed in our clinical samples. Blue light activates PpIX well in superficial tissues (like skin cancers) but gets absorbed quickly, whereas red light penetrates deeper but activates less efficiently at its peak, requiring more power but reaching more tissue. PpIX strongly absorbs blue light (Soret band at ~410 nm), generating reactive oxygen species efficiently. Blue light penetrates less than 1 mm into tissue, making it excellent for very shallow skin cancers (like basal cell or actinic keratoses) and surface lesions. It is not suitable for solid tumors or deeper malignancies because it does not reach them. So, 410 nm is specific to superficial applications, while red light is better for deeper, more challenging cancers. A 2023 review in Photochemistry and Photobiology evaluates the progression of PDT for bladder cancer, highlighting developments in photosensitizers and delivery techniques since its initial approval in 1993 [51]. PDT is increasingly viewed as a viable focal therapy for low-to-intermediate-risk localized disease. It offers high precision with minimal damage to healthy tissues, such as the neurovascular bundles, which helps preserve erectile and urinary function [66]. While still under investigation as a primary treatment, PDT is being explored as an alternative for cases resistant to traditional therapies [67]. While PpIX [51] and RB are not currently the "standard of care" for clinical bladder PDT, researchers use them in experimental models to address critical failures of traditional therapies like Photofrin and ALA-PDT [32].

5. Conclusions

This study provides preliminary microscopic evidence for the potential efficacy of PDT in LG pTa NMIBC tissue in an ex vivo model. The observed histopathological changes, such as chromatin condensation, pyknosis, and nuclear fragmentation, suggest the induction of apoptotic processes dependent on the photosensitizer concentration. The use of frozen tissue (cryosection) in PDT research also has some positive and negative aspects that may equally affect the results compared to living tissue. Given these results, these photosensitizers are highly suited for superficial applications, such as endoscopic treatment of early-stage lesions or antibacterial therapy. The use of frozen tissues is justified in the initial phase for precise optical and chemical mapping; however, the full picture of PDT efficacy in bladder cancer (including vascular and immunological effects) requires verification in

living models. Further research with larger cohorts is planned to confirm these pilot data and move toward definitive clinical protocols.

Author Contributions: Conceptualization, D.G., M.O. and D.A.; methodology, D.G., M.O. and D.A.; formal analysis, D.G., M.O. and D.A.; investigation, T.K., A.P. and S.C.; writing—original draft preparation, D.G.; writing—review and editing, D.G., M.O., T.K. and D.A.; visualization, A.P. and S.C.; supervision, T.K. and D.A.; project administration, D.G., M.O., T.K. and D.A.; funding acquisition, T.K. and D.A. All authors have read and agreed to the published version of the manuscript.

Funding: This research received no external funding.

Institutional Review Board Statement: The study was conducted in accordance with the Declaration of Helsinki, and approved by the Ethics Committee of the University of Rzeszów. (Approval Code: 29/05/2019, Approval date: 9 May 2019).

Informed Consent Statement: Informed consent was obtained from all subjects involved in the study.

Data Availability Statement: The original contributions presented in this study are included in the article. Further inquiries can be directed to the corresponding authors.

Conflicts of Interest: The authors declare no conflicts of interest.

References

1. Cancer Today. Available online: https://gco.iarc.who.int/today/ (accessed on 6 May 2025).
2. Leslie, S.W.; Soon-Sutton, T.L.; Aeddula, N.R. Bladder Cancer. In *StatPearls [Internet]*; StatPearls Publishing: Treasure Island, FL, USA, January 2025. Available online: https://www.ncbi.nlm.nih.gov/books/NBK536923/ (accessed on 14 April 2026).
3. Soares, A.; Bourlon, M.T.; Wong, A.; Joshi, A.; Jardim, D.; Korbenfeld, E.; Karak, F.E.; Orlandi, F.; Sze, H.; Ansari, J.; et al. Management of Metastatic Urothelial Carcinoma in Emerging Markets (EM): An Expert Opinion. *Clin. Genitourin. Cancer* **2024**, *22*, 467–475. [CrossRef]
4. Aldousari, S.; Kassouf, W. Update on the management of non-muscle invasive bladder cancer. *Can. Urol. Assoc. J.* **2010**, *4*, 56–64. [CrossRef] [PubMed]
5. Brierley, J.D.; Gospodarowicz, M.K.; Wittekind, C. *TNM Classification of Malignant Tumours*; John Wiley & Sons: Hoboken, NJ, USA, 2017.
6. Ro, J.Y.; Staerkel, G.A.; Ayala, A.G. Cytologic and histologic features of superficial bladder cancer. *Urol. Clin. N. Am.* **1992**, *19*, 435–453. [CrossRef]
7. Daza, J.; Grauer, R.; Chen, S.; Lavallèe, E.; Razdan, S.; Dey, L.; Steineck, G.; Renström-Koskela, L.; Li, Q.; Hussein, A.A.; et al. Development of a predictive model for recurrence-free survival in pTa low-grade bladder cancer. *Urol. Oncol. Semin. Orig. Investig.* **2023**, *41*, 256.e9–256.e15. [CrossRef] [PubMed]
8. Jeong, S.; Han, J.H.; Jeong, C.W.; Kim, H.H.; Kwak, C.; Yuk, H.D.; Ku, J.H. Clinical determinants of recurrence in pTa bladder cancer following transurethral resection of bladder tumor. *BMC Cancer* **2022**, *22*, 631. [CrossRef]
9. Waidelich, R.; Stepp, H.; Baumgartner, R.; Weninger, E.; Hofstetter, A.; Kriegmair, M. Clinical experience with 5-aminolevulinic acid and photodynamic therapy for refractory superficial bladder cancer. *J. Urol.* **2001**, *165*, 1904–1907. [CrossRef]
10. Kwiatkowski, S.; Knap, B.; Przystupski, D.; Saczko, J.; Kędzierska, E.; Knap-Czop, K.; Kotlińska, J.; Michel, O.; Kotowski, K.; Kulbacka, J. Photodynamic therapy—Mechanisms, photosensitizers and combinations. *Biomed. Pharmacother.* **2018**, *106*, 1098–1107. [CrossRef] [PubMed]
11. Khan, N.H.; Mir, M.; Qian, L.; Baloch, M.; Ali Khan, M.F.; Rehman, A.U.; Ngowi, E.E.; Wu, D.D.; Ji, X.Y. Skin cancer biology and barriers to treatment: Recent applications of polymeric micro/nanostructures. *J. Adv. Res.* **2022**, *36*, 223–247. [CrossRef]
12. Ramsay, D.; Stevenson, H.; Jerjes, W. From Basic Mechanisms to Clinical Research: Photodynamic Therapy Applications in Head and Neck Malignancies and Vascular Anomalies. *J. Clin. Med.* **2021**, *10*, 4404. [CrossRef]
13. Wang, H.; Ewetse, M.P.; Ma, C.; Pu, W.; Xu, B.; He, P.; Wang, Y.; Zhu, J.; Chen, H. The 'Light Knife' for Gastric Cancer: Photodynamic Therapy. *Pharmaceutics* **2022**, *15*, 101. [CrossRef]
14. Hanada, Y.; Pereira, S.P.; Pogue, B.; Maytin, E.V.; Hasan, T.; Linn, B.; Mangels-Dick, T.; Wang, K.K. EUS-guided verteporfin photodynamic therapy for pancreatic cancer. *Gastrointest. Endosc.* **2021**, *94*, 179–186. [CrossRef]
15. Li, Y.; Yan, B.; He, S. Advances and challenges in the treatment of lung cancer. *Biomed. Pharmacother.* **2023**, *169*, 115891. [CrossRef] [PubMed]

16. Xue, Q.; Zhang, J.; Jiao, J.; Qin, W.; Yang, X. Photodynamic therapy for prostate cancer: Recent advances, challenges and opportunities. *Front. Oncol.* **2022**, *12*, 980239. [CrossRef]
17. Dyrskjøt, L.; Hansel, D.E.; Efstathiou, J.A.; Knowles, M.A.; Galsky, M.D.; Teoh, J.; Theodorescu, D. Bladder cancer. *Nat. Rev. Dis. Primers* **2023**, *9*, 58. [CrossRef]
18. Kubrak, T.; Karakuła, M.; Czop, M.; Kawczyk-Krupka, A.; Aebisher, D. Advances in Management of Bladder Cancer—The Role of Photodynamic Therapy. *Molecules* **2022**, *27*, 731. [CrossRef] [PubMed]
19. Zhao, T.; Song, J.; Ping, Y.; Li, M. The Application of Antimicrobial Photodynamic Therapy (aPDT) in the Treatment of Peri-Implantitis. *Comput. Math. Methods Med.* **2022**, *2022*, 3547398. [CrossRef] [PubMed]
20. Allison, R.R.; Moghissi, K. Photodynamic Therapy (PDT): PDT Mechanisms. *Clin. Endosc.* **2013**, *46*, 24–29. [CrossRef]
21. Brundish, D.E.; Love, W.G. Photodynamic therapy comes of age. *IDrugs* **2000**, *3*, 1487–1508.
22. Castano, A.P.; Demidova, T.N.; Hamblin, M.R. Mechanisms in photodynamic therapy: Part two-cellular signaling, cell metabolism and modes of cell death. *Photodiagn. Photodyn. Ther.* **2005**, *2*, 1–23. [CrossRef]
23. Nowak-Stepniowska, A.; Pergoł, P.; Padzik-Graczyk, A. Photodynamic method of cancer diagnosis and therapy—Mechanisms and applications. *Postep. Biochem.* **2003**, *59*, 53–63.
24. Plaetzer, K.; Krammer, B.; Berlanda, J.; Berr, F.; Kiesslich, T. Photophysics and photochemistry of photodynamic therapy: Fundamental aspects. *Lasers Med. Sci.* **2009**, *24*, 259–268. [CrossRef]
25. Juzeniene, A.; Moan, J. The history of PDT in Norway Part one: Identification of basic mechanisms of general PDT. *Photodiagn. Photodyn. Ther.* **2007**, *4*, 3–11. [CrossRef]
26. Fonseca, S.M.; Pina, J.; Arnaut, L.G.; Seixas de Melo, J.; Burrows, H.D.; Chattopadhyay, N.; Alcacer, L.; Charas, A.; Morgado, J.; Monkman, A.P.; et al. Triplet-state and singlet oxygen formation in fluorene-based alternating copolymers. *J. Phys. Chem. B* **2006**, *110*, 8278–8283. [CrossRef] [PubMed]
27. Garg, A.D.; Nowis, D.; Golab, J.; Agostinis, P. Photodynamic therapy: Illuminating the road from cell death towards anti-tumour immunity. *Apoptosis* **2010**, *15*, 1050–1071. [CrossRef] [PubMed]
28. Ethirajan, M.; Chen, Y.; Joshi, P.; Pandey, R.K. The role of porphyrin chemistry in tumor imaging and photodynamic therapy. *Chem. Soc. Rev.* **2011**, *40*, 340–362. [CrossRef]
29. Li, J.-W.; Wu, Z.-M.; Magetic, D.; Zhang, L.-J.; Chen, Z.-L. Antitumor effects evaluation of a novel porphyrin derivative in photodynamic therapy. *Tumor Biol.* **2015**, *36*, 9685–9692. [CrossRef] [PubMed]
30. Zhang, L.-J.; Yan, Y.-J.; Liao, P.-Y.; Margetic, D.; Wang, L.; Chen, Z.-L. Synthesis and antitumor activity evaluation of a novel porphyrin derivative for photodynamic therapy in vitro and in vivo. *Tumor Biol.* **2016**, *37*, 6923–6933. [CrossRef]
31. Beiki, D.; Eggleston, I.M.; Pourzand, C. Daylight-PDT: Everything under the sun. *Biochem. Soc. Trans.* **2022**, *50*, 975–985. [CrossRef]
32. Lefebvre, A.; Marhfor, S.; Baert, G.; Deleporte, P.; Grolez, G.P.; Boileau, M.; Morales, O.; Vignoud, S.; Delhem, N.; Mortier, L.; et al. Photodynamic Therapy Using a Rose-Bengal Photosensitizer for Hepatocellular Carcinoma Treatment: Proposition for a Novel Green LED-Based Device for In Vitro Investigation. *Biomedicines* **2024**, *12*, 2120. [CrossRef]
33. Ash, C.; Dubec, M.; Donne, K.; Bashford, T. Effect of wavelength and beam width on penetration in light-tissue interaction using computational methods. *Lasers Med. Sci.* **2017**, *32*, 1909–1918. [CrossRef]
34. Bissoyi, A.; Nayak, B.; Pramanik, K.; Sarangi, S.K. Targeting cryopreservation-induced cell death: A review. *Biopreserv. Biobank.* **2014**, *12*, 23–34. [CrossRef] [PubMed]
35. Chow-Shi-Yée, M.; Grondin, M.; Ouellet, F.; Averill-Bates, D.A. Control of stress-induced apoptosis by freezing tolerance-associated wheat proteins during cryopreservation of rat hepatocytes. *Cell Stress Chaperones* **2020**, *25*, 869–886. [CrossRef]
36. Whaley, D.; Damyar, K.; Witek, R.P.; Mendoza, A.; Alexander, M.; Lakey, J.R. Cryopreservation: An Overview of Principles and Cell-Specific Considerations. *Cell Transplant.* **2021**, *30*, 963689721999617. [CrossRef] [PubMed]
37. Cummings, B.S.; Schnellmann, R.G. Measurement of cell death in mammalian cells. *Curr. Protoc. Pharmacol.* **2004**, *25*, 12.8.1–12.8.22. [CrossRef] [PubMed]
38. Schäfer, A.T.; Kaufmann, J.D. What happens in freezing bodies?: Experimental study of histological tissue change caused by freezing injuries. *Forensic Sci. Int.* **1999**, *102*, 149–158. [CrossRef]
39. Hubel, A.; Spindler, R.; Skubitz, A.P.N. Storage of Human Biospecimens: Selection of the Optimal Storage Temperature. *Biopreserv. Biobank.* **2014**, *12*, 165–175. [CrossRef]
40. Esteva-Socias, M.; Artiga, M.J.; Bahamonde, O.; Belar, O.; Bermudo, R.; Castro, E.; Escámez, T.; Fraga, M.; Jauregui-Mosquera, L.; Novoa, I.; et al. In search of an evidence-based strategy for quality assessment of human tissue samples: Report of the tissue Biospecimen Research Working Group of the Spanish Biobank Network. *J. Transl. Med.* **2019**, *17*, 370. [CrossRef]
41. Aebisher, D.; Osuchowski, M.; Bartusik-Aebisher, D.; Krupka-Olek, M.; Dynarowicz, K.; Kawczyk-Krupka, A. An Analysis of the Effects of In Vitro Photodynamic Therapy on Prostate Cancer Tissue by Histopathological Examination and Magnetic Resonance Imaging. *Int. J. Mol. Sci.* **2022**, *23*, 11354. [CrossRef] [PubMed] [PubMed Central]

42. Ostańska, E.; Barnaś, E.; Bartusik-Aebisher, D.; Dynarowicz, K.; Szpunar, M.; Skręt-Magierło, J.; Aebisher, D. Histopathological Analysis of the Effect of Photodynamic Action on Post-Chemotherapy Excised Breast Cancer Tissue. *Medicina* **2022**, *58*, 700. [CrossRef] [PubMed] [PubMed Central]
43. Godlewski, D.; Dynarowicz, K.; Truszkiewicz, A.; Osuchowski, M.; Kubrak, T.; Bartusik-Aebisher, D.; Przygórzewska, A.; Szpara, J.; Aebisher, D. Assessment of T1 and T2 Relaxation-Time Changes in NMIBC Tissue After 5-ALA Photodynamic Therapy Using Quantitative Magnetic Resonance Imaging. *Biomedicines* **2025**, *13*, 2867. [CrossRef]
44. Przygoda, M.; Bartusik-Aebisher, D.; Dynarowicz, K.; Cieślar, G.; Kawczyk-Krupka, A.; Aebisher, D. Cellular Mechanisms of Singlet Oxygen in Photodynamic Therapy. *Int. J. Mol. Sci.* **2023**, *24*, 16890. [CrossRef] [PubMed]
45. Arnaut, L.G.; Schaberle, F.A.; Sereno, J.; Gomes-da-Silva, L.C. Flash Photodynamic Therapy—How the Saturation of Photosensitizer Absorption Enables Selective and DeeperTumor Treatments. *Adv. Sci.* **2026**, *13*, e13199. [CrossRef] [PubMed]
46. Ziegler, U.; Groscurth, P. Morphological Features of Cell Death. *Physiology* **2024**, *19*, 124–128. [CrossRef]
47. Tonnus, W.; Meyer, C.; Paliege, A.; Belavgeni, A.; von Mässenhausen, A.; Bornstein, S.R.; Hugo, C.; Becker, J.U.; Linkermann, A. The pathological features of regulated necrosis. *J. Pathol.* **2019**, *247*, 697–707. [CrossRef]
48. Heng, B.C.; Ye, C.P.; Liu, H.; Toh, W.S.; Rufaihah, A.J.; Yang, Z.; Bay, B.H.; Ge, Z.; Ouyang, H.W.; Lee, E.H.; et al. Loss of viability during freeze-thaw of intact and adherent human embryonic stem cells with conventional slow-cooling protocols is predominantly due to apoptosis rather than cellular necrosis. *J. Biomed. Sci.* **2006**, *13*, 433–445. [CrossRef] [PubMed]
49. Landes, R.; Illanes, A.; Goeppner, D.; Gollnick, H.; Friebe, M. A study of concentration changes of Protoporphyrin IX and Coproporphyrin III in mixed samples mimicking conditions inside cancer cells for Photodynamic Therapy. *PLoS ONE* **2018**, *13*, e0202349. [CrossRef]
50. Chen, Z.; Li, W.; Hu, X.; Liu, M. Irradiance plays a significant role in photobiomodulation of B16F10 melanoma cells by increasing reactive oxygen species and inhibiting mitochondrial function. *Biomed. Opt. Express* **2019**, *11*, 27–39. [CrossRef]
51. Rahman, K.M.M.; Giram, P.; Foster, B.A.; You, Y. Photodynamic Therapy for Bladder Cancers, A Focused Review. *Photochem. Photobiol.* **2023**, *99*, 420–436. [CrossRef]
52. Arum, C.J.; Gederaas, O.A.; Krokan, H.E.; Chen, D.; Zhao, C.M.; Larsen, E.L.P.; Randeberg, L.L.; Svaasand, L.O.; Hjelde, A. Tissue responses to hexyl 5-aminolevulinate-induced photodynamic treatment in syngeneic orthotopic rat bladder cancer model: Possible pathways of action. *J. Biomed. Opt.* **2011**, *16*, 028001. [CrossRef]
53. Grönlund-Pakkanen, S.; Wahlfors, J.; Talja, M.; Kosma, V.M.; Pakkanen, T.M.; Ala-Opas, M.; Alhava, E.; Moore, R.B. The effect of photodynamic therapy on rat urinary bladder with orthotopic urothelial carcinoma. *BJU Int.* **2003**, *92*, 125–130. [CrossRef]
54. Bronshtein, I.; Afri, M.; Weitman, H.; Frimer, A.A.; Smith, K.M.; Ehrenberg, B. Porphyrin Depth in Lipid Bilayers as Determined by Iodide and Parallax Fluorescence Quenching Methods and Its Effect on Photosensitizing Efficiency. *Biophys. J.* **2004**, *87*, 1155–1164. [CrossRef]
55. Li, B.; Shen, Y.; Lin, H.; Wilson, B.C. Correlation of in vitro cell viability and cumulative singlet oxygen luminescence from protoporphyrin IX in mitochondria and plasma membrane. *Photodiagn. Photodyn. Ther.* **2024**, *46*, 104080. [CrossRef]
56. Ji, Z.; Yang, G.; Vasovic, V.; Cunderlikova, B.; Suo, Z.; Nesland, J.M.; Peng, Q. Subcellular localization pattern of protoporphyrin IX is an important determinant for its photodynamic efficiency of human carcinoma and normal cell lines. *J. Photochem. Photobiol. B* **2006**, *84*, 213–220. [CrossRef] [PubMed]
57. Demartis, S.; Obinu, A.; Gavini, E.; Giunchedi, P.; Rassu, G. Nanotechnology-based rose Bengal: A broad-spectrum biomedical tool. *Dye. Pigment.* **2021**, *188*, 109236. [CrossRef]
58. Sztandera, K.; Gorzkiewicz, M.; Zizzi, E.A.; Dybczak, N.; Poltorak, L.; Deriu, M.A.; Klajnert-Maculewicz, B. Cellular uptake of rose bengal is mediated by OATP1B1/1B3 transporters. *Bioelectrochemistry* **2023**, *152*, 108449. [CrossRef]
59. Bacellar, I.O.L.; Baptista, M.S. Mechanisms of Photosensitized Lipid Oxidation and Membrane Permeabilization. *ACS Omega* **2019**, *4*, 21636–21646. [CrossRef]
60. Ruhi, M.K. Protoporphyrin IX Beyond Conventional Applications: A Review of Emerging Research Directions. *Life* **2025**, *15*, 1516. [CrossRef] [PubMed]
61. Manivasager, V.; Yee, K.K.; Heng, P.W.; Soo, K.C.; Olivo, M. A study comparing endogenous protoporphyrin IX induced by 5-ALA and ALA-methyl ester with exogenous PpIX and PpIX dimethyl ester in photodynamic diagnosis of human nasopharyngeal carcinoma xenografts. *Int. J. Oncol.* **2006**, *29*, 997–1002. [CrossRef] [PubMed]
62. Alekseeva, P.M.; Efendiev, K.T.; Shiryaev, A.A.; Rusakov, M.A.; Simonova, M.S.; Samoylova, S.I.; Fatyanova, A.S.; Reshetov, I.V.; Loschenov, V.B. Sublingual administration of 5-aminolevulinic acid for laser-induced photodiagnostics and photodynamic therapy of oral cavity and larynx cancers. *Photodiagn. Photodyn. Ther.* **2021**, *34*, 102289. [CrossRef]
63. Aebisher, D.; Woźnicki, P.; Bartusik-Aebisher, D. Photodynamic Therapy and Adaptive Immunity Induced by Reactive Oxygen Species: Recent Reports. *Cancers* **2024**, *16*, 967. [CrossRef]
64. Krammer, B. Vascular effects of photodynamic therapy. *Anticancer Res.* **2001**, *21*, 4271–4277.
65. Ormond, A.B.; Freeman, H.S. Dye Sensitizers for Photodynamic Therapy. *Materials* **2013**, *6*, 817–840. [CrossRef]

66. Fukuhara, H.; Yamamoto, S.; Karashima, T.; Inoue, K. Photodynamic diagnosis and therapy for urothelial carcinoma and prostate cancer: New imaging technology and therapy. *Int. J. Clin. Oncol.* **2021**, *26*, 18–25. [CrossRef]
67. Pogue, B.W.; Chen, B.; Ochoa, M.I.; Petusseau, A.; Liu, A.; Gibson, A.L.F.; Maytin, E.V.; Wilson, B.C. Emerging uses of 5-aminolevulinic-acid-induced protoporphyrin IX in medicine: A review of multifaceted, ubiquitous, molecular diagnostic, therapeutic, and theranostic opportunities. *J. Biomed. Opt.* **2025**, *30*, S34112. [CrossRef]

Disclaimer/Publisher's Note: The statements, opinions and data contained in all publications are solely those of the individual author(s) and contributor(s) and not of MDPI and/or the editor(s). MDPI and/or the editor(s) disclaim responsibility for any injury to people or property resulting from any ideas, methods, instructions or products referred to in the content.